Published in final edited form as:
*Anal Chem*. 2010 November 15; 82(22): 9357–9364. doi:10.1021/ac101977f.

# Microchannel-Nanopore Device for Bacterial Chemotaxis Assays

**Michelle L. Kovarik**[§], **Pamela J. B. Brown**[‡], **David T. Kysela**[‡], **Cécile Berne**[‡], **Anna C. Kinsella**[§], **Yves V. Brun**[‡], and **Stephen C. Jacobson**[*,§]

[§] Department of Chemistry, Indiana University, Bloomington, IN 47405

[‡] Department of Biology, Indiana University, Bloomington, IN 47405

## Abstract

Motile bacteria bias the random walk of their motion in response to chemical gradients by the process termed chemotaxis, which allows cells to accumulate in favorable environments and disperse from less favorable ones. In this work, we describe a simple microchannel-nanopore device that establishes a stable chemical gradient for chemotaxis assays in ≤ 1 min. Chemoattractant is dispensed by diffusion through 10 nm diameter pores at the intersection of two microchannels. This design requires no external pump and minimizes the effect of transmembrane pressure, resulting in a stable, reproducible gradient. The microfluidic platform facilitates microscopic observation of individual cell trajectories, and chemotaxis is quantified by monitoring changes in cell swimming behavior in the vicinity of the intersection. We validate this system by measuring the chemotactic response of an aquatic bacterium, *Caulobacter crescentus*, to xylose concentrations from 1.3 μM to 1.3 M. Additionally, we make an unanticipated observation of increased turn frequency in a chemotaxis-impaired mutant which provides new insight into the chemotaxis pathway in *C. crescentus*.

Swimming bacteria sense changes in the concentration of chemicals in their environment and respond with distinct changes in swimming behavior. This process, termed chemotaxis, allows bacteria to bias the random walk of their motion in order to accumulate in favorable environments and disperse from less favorable environments. The flagellum-mediated motion of a bacterium alternates between straight runs, during which the flagellum (or multiple flagella) rotates clockwise or counterclockwise depending the microorganism, and turns, during which the flagellum reverses its rotation direction.[1,2] Switching of flagellar rotation reorients the cell in a random new direction and results in tumbles for many bacteria, such as *Escherichia coli*, or brief reversals in swimming direction for others, such as *Caulobacter crescentus*.[3–5] Binding of chemoattractant molecules to receptors on the cell surface suppresses flagellar switching, allowing the bacterium to travel up a chemical gradient toward higher attractant concentrations.[6,7]

The aquatic bacterium *Caulobacter crescentus* has potential utility in bioremediation, and chemotaxis can play a major role in bioremediation. If a microorganism is able to sense a toxin and move up its concentration gradient, efficient degradation of that toxin by the microorganism is possible.[8] The chemotactic ability of some bacteria has been shown to help them approach and degrade toxic compounds in the environment,[8–10] and the well-documented hardiness[11–18] of *C. crescentus* makes it a potential candidate of choice for these purposes. However, a thorough understanding of how *C. crescentus* senses and

[*]Corresponding author. jacobson@indiana.edu.

Supporting Information Available. Video of cells swimming in the microfluidic device; details of microfluidic device fabrication, swarmer enrichment assay, agar plate studies, and MPTS dye compatibility; tables of run length and duration data for the wild type and mutant strains; and histograms of the mutant data. This material is available free of charge via the Internet at http://pubs.acs.org.

responds to well-known and characterized chemoattractants is required before engineering a strain capable of a chemotactic response toward toxins. The first study of chemotaxis in *C. crescentus* was published more than twenty years ago,[19] yet the exact biochemical mechanism and the full array of chemoattractants remain unknown. Miniaturized instrumentation for chemotaxis assays presents a number of advantages. For assays of chemotaxis toward toxic compounds, the small volumes required limit the amount of hazardous material handled. Furthermore, the relative rapidity of these assays compared to more traditional methods improves throughput compared to traditional chemotactic assays, which require hours or days.[20,21] A rapid assay would be particularly advantageous for studies of *C. crescentus*, which is only motile and capable of chemotaxis for part of its life cycle.[11]

Microfluidic systems are also well-suited to studies of bacterial chemotaxis because of their precise fluid handling and micrometer to millimeter length scale. Microchannel plumbing can readily establish reproducible and often complex chemical gradients in space and time,[22–25] and the lateral dimensions of microchannels permit accurate tracking of individual bacterial cells (typically 0.5–3 μm) in a reasonable field of view. To date, several microfluidic platforms have been reported for studies of microbial chemotaxis,[20,21,26–31] aerotaxis,[32] and thermotaxis.[33] In two cases, results from microfluidic devices demonstrated sensitivity of an organism to chemoattractant concentrations several orders of magnitude below the detection limit identified with traditional assays.[20,21]

Microfluidic devices designed for bacterial chemotaxis assays generally fall into one of two groups: those that rely on flow to develop a chemical gradient and those based solely on diffusion. Flow-based devices typically use a channel intersection to mix plain media or buffer with a chemoattractant.[20,26,27] After laminar streams are combined, a gradient is established as chemoattractant diffuses laterally across the channel. Diffusive gradients may be created laterally[28] or axially.[21,29] Several generations of source-sink devices have been demonstrated for chemotaxis studies.[30,31,34–36] Each of these devices generates a stable chemical gradient, but the time for gradient formation depends on the distance from sink to source and ranges from 10 min[31] up to 6 h.[34]

In this work, we describe a diffusion-based device that generates a stable, reproducible gradient in ≤1 min. The device design used is shown in Figure 1 and consisted of two poly(dimethylsiloxane) (PDMS) channels in separate device layers, placed orthogonally to one another and bridged by a commercially available track-etch nanopore membrane. Although this geometry has been used previously to control mass transport in microfluidic devices,[37,38] we report device utility in chemical gradient formation, including choice of nanopore diameter and characterization of the time required for gradient formation, gradient stability, and gradient reproducibility from device to device. The design was validated by studying the response of individual wild type and a chemotaxis-impaired mutant cells of *C. crescentus* to a known chemoattractant, xylose (see Supporting Information).[19] The life cycle of *C. crescentus* includes only a brief window of motility (e.g., 30–60 min), and the single cell measurements reported here benefit from interrogating large sample sizes during the motility window. Consequently, this application highlights the advantages of a compact microchannel structure that permits rapid gradient formation and accurate tracking of motile cells with moderate swim velocities, e.g., ~30 μm/s.

## Experimental Section

### Device fabrication

Multilayer microfluidic devices for the chemotaxis assays were assembled from PDMS microchannels and track-etch nanopore membranes as described previously.[39] Fabrication

details are given in the Supporting Information. The resulting PDMS channels were each a single straight line, 110 ± 2 μm wide, 19.1 ± 0.1 μm deep, and 1 cm long. The two channels were bridged at the intersection by 10 nm diameter cylindrical pores in a polycarbonate track-etch membrane (GE Osmonics, Inc.).

## Cell preparation

*C. crescentus* has a dimorphic life cycle (see Figure S-1) in which each cell division gives rise to two genetically identical but morphologically distinct daughter cells: a non-motile stalked cell capable of cell division and a non-reproductive motile swarmer cell with a single polar flagellum and pili. Because only motile cells are capable of chemotaxis, cultures for these experiments were enriched in swarmer cells using a modified plate releasing technique described in the Supporting Information.[40] Typically, the enriched culture consisted of 80–95% swarmer cells.

Two strains of *C. crescentus* were used in these experiments, CB15Tn*7gfp3* (YB4789) and CB15Δ*cheA*Tn*7gfp3* (YB5097). CB15 is wild type *C. crescentus*, and CB15Δ*cheA* is a chemotaxis-impaired mutant that lacks the *cheA* (CC0433) gene. Both strains were genetically modified with a transposon, pBK-mini-Tn*7gfp3*,[41] to constitutively express cytoplasmic green fluorescent protein (GFP). Details concerning the construction and GFP-labeling of these strains are included in the Supporting Information.

## Chemotaxis assays

The microchannels were filled with M2G, a standard minimal growth media for *C. crescentus*,[42] by applying a subambient pressure from a house vacuum line. Appropriate flow conditions were then established by filling the reservoirs with 85, 90, 95 and 100 μL of M2G, starting with the cell outlet (reservoir 3) and proceeding counterclockwise around the device to the sample inlet (reservoir 4). M2G spiked with 10 μM 8-methoxypyrene-1,3,5-trisulfonic acid (MPTS; Sigma-Aldrich) was added to the sample inlet reservoir as a fluorescent tracer. Approximately 5 μL of concentrated, enriched swarmer cells, prepared as described above, were added to the cell inlet (reservoir 1), and the reservoir levels were adjusted to achieve a flow velocity of 15–30 μm/s in the cell channel. After control data had been recorded, the contents of the sample reservoir were replaced with a chemoattractant solution, and hydrostatic flow in the sample channel carried the chemoattractant solution from the reservoir to the intersection within 30–60 s. The gradient was then rapidly established by diffusion through the membrane.

An inverted optical microscope (TE-2000U, Nikon, Inc.) equipped for epifluorescence, a 20× objective, CCD camera (9100-13, Hamamatsu Corp.), and IPLab software (BD Biosciences) were used to monitor individual swarmer cells for the chemotaxis assays. Fluorescein isothiocyanate and coumarin filter cubes (96320M and 31047v2, Nikon, Inc.) were used to obtain the GFP and MPTS fluorescence signals, respectively. A Nikon C1 scanning confocal microscope with a 40× Plan Fluor extra-long working distance objective (NA = 0.6; Nikon, Inc.) was used to take confocal images of fluorescein diffusion in an assembled device.

Video data were recorded by streaming 301 frames at a frame rate of 10.9 – 13.9 fps. As a control, videos of cell swimming were recorded in the absence of chemoattractant in the sample channel. As noted above, after the baseline cell swimming behavior was established, the contents of the sample inlet (reservoir 4) were replaced with a solution of the chemoattractant, xylose, and 10 μM MPTS in M2G. Xylose is one of the most well-studied chemoattractants for *C. crescentus*[16] and produced a particularly strong chemotactic response relative to other sugars in traditional swarm plate assays (data not shown). Xylose

at 13 mM (0.2% w/v) was used for preliminary assays because this concentration is the standard for *C. crescentus* cultures[11,42] and was used for previous swarm plate assays (see Supporting Information).[16] Subsequent assays were performed by varying this initial concentration (1.3 μM, 130 μM, and 1.3 M) to demonstrate the wide dynamic ranges of both the assay and bacterial chemotaxis pathway. The MPTS fluorescence signal at the intersection was checked before and after replacing the sample solution to ensure no major change occurred in the gradient. After allowing a minimum of 2 min for the gradient to form, videos were obtained of the cell response to the chemoattractant.

## Data analysis

A combination of freely-available ImageJ software and custom-written MATLAB programs (The MathWorks, Inc.) was used to analyze the video data. The ParticleTracker plug-in[43] for Image J was used to obtain trajectory coordinates for each cell. This plug-in required five input parameters to determine the cell trajectories: radius, cut-off, intensity percentile, displacement, and link range. Radius refers to the size, in pixels, of a single cell and was set to 5 for all videos. The cut-off value discriminates against aggregates on the basis of their $0^{th}$ and $2^{nd}$ intensity moments. No aggregates were observed in these experiments, and this value was set to 0 for all analyses. The intensity percentile varied from 0.05% to 1.2%, meaning that particles in the top 0.05% to 1.2% of the intensity range for a given video were identified as cells. This value varied depending on background intensity, cell density, and presence of adhered cells in the field of view. Displacement refers to the maximum number of pixels a cell can travel between frames and was set to 12–15. The link range is the number of subsequent frames the plug-in examines to find the next position of a cell. For example, a link range of 1 means that a cell identified in frame 1 must be found in frame 2 for the trajectory to continue. A link range of 2 means that a cell identified in frame 1 could go unidentified in frame 2, perhaps because the cell had gone out of the focal plane, but be identified in frame 3. Link ranges of 1–3 were used in these analyses, and any trajectories containing spurious links were readily identified and deleted.

A custom MATLAB program was used to extract the relevant statistics about cell motion from the trajectories. To improve data quality, this program first disregarded all trajectories < 100 μm long or for which cell position deviated less than 5 μm from the starting point (i.e., adhered cells). Trajectories were then discriminated as either swimming or non-swimming (dead or non-motile stalked) cells. Cells were identified as non-swimming if ≥ 95% of the total accumulated distance traveled was in the direction of flow. These trajectories were used to determine the flow rate. Cell trajectories with ≤ 90% of motion in the direction of flow were analyzed as swimming cells, and all trajectories for which 90% to 95% of cell motion was with the flow were not considered because of difficulty determining which of these tracks corresponded to non-swimming cells and which to swimming cells following the channel wall.

For swimming cell trajectories, the MATLAB program determined the length and duration of each run nested between two reversals, or turns. To identify turns, the angle formed by each triplet of consecutive points was calculated. A point in the trajectory was considered a turn when the difference between two consecutive angles was ≥ 90°. Ignoring points where the change in angle with time was < 90° eliminated identification of circling paths as strings of turns.

*C. crescentus* swarmer cells have long, thin filaments called pili at their flagellar pole that promote cell adhesion to surfaces (see Figure S-1).[44,45] In these experiments, cells occasionally adhered to the channel, spun around their flagella, released from the surface, and swam away in another direction. Chemotaxis is indicated by a change in direction caused by reversal of the flagellum motor. To avoid identifying changes in swim direction

after release from a surface as turns, cells were required to travel at least 1 μm away from a turn location within 4 frames of the turn. Otherwise, that point was identified as a "false turn" where the cell temporarily adhered to the channel and was not used in any run length or duration calculations.

## Results and Discussion

### Gradient tracking

Gradient formation and stability were monitored with MPTS, a blue fluorescent, pyrene-based dye with a net charge of −3. This charge makes the dye hydrophilic and prevented adsorption into the PDMS channels (a common problem with more hydrophobic dyes, such as Rhodamine B).[46] Using this blue dye instead of the more commonly used fluorescein allowed us to track the gradient in real-time during experiments without obscuring the GFP signal from the bacterial cells. Because we found no literature reports of MPTS used in cell-based assays, we conducted agar plate studies to confirm that MPTS was not cytotoxic, could not be used by *C. crescentus* as a carbon source and did not interfere with chemotaxis toward xylose. Details of the agar plate studies performed are included in the Supporting Information, and the results are shown in Figures S-2 and S-3.

Figure 2 shows a fluorescence image of the device intersection with the sample channel filled with 10 μM MPTS in M2G and the cell channel with M2G. The line profile shows the average fluorescence signal in the cell channel (vertical) minus the average fluorescence from the areas immediately to the left and right of the cell channel. The result is that the average fluorescence from the sample channel is subtracted from the signal at the intersection, and the remaining maximum in the line profile indicates the patch of chemoattractant encountered by cells at the intersection. While the xylose concentration could not be imaged directly, the diffusion coefficient of MPTS, estimated as $3.3 \times 10^{-6}$ $cm^2/s$ (that of the hydroxyl analogue, 8-hydroxypyrene-1,3,5-trisulfonic acid)[47] is approximately 45% that of xylose, making MPTS a reasonably good tracer for xylose diffusion.

In order to characterize the shape of the gradient, confocal imaging was attempted with a Nikon C1 scanning confocal microscope. The sample channel was filled with fluorescein (100 nM or 10 μM), and the cell channel was filled with M2G buffer solution. Unfortunately, the low concentration of material in the cell channel relative to the sample channel resulted in high background for both fluorescein concentrations despite the confocal setup. The amount of material transferred across the membrane was very low, as evidenced by the absence of any discernible increase in signal below the intersection compared to the cell channel area upstream. This issue was exacerbated by the long working distance required to focus through the PDMS substrate onto the membrane (e.g., ~1.5 mm), which resulted in poor discrimination of light in the z-direction. As a result, useful confocal images were not obtained, and subsequent characterization of the gradient was performed by epifluorescence microscopy.

### Gradient formation and stability

Gradient formation in the device was rapid due to the short distance over which the chemoattractant diffused (6 μm membrane thickness plus 19 μm channel depth). This represents one advantage over previous membrane-based devices which required chemoattractant to diffuse laterally across the channel or axially down its length, resulting in much longer gradient formation times.[30,31,34,36] In the device presented here, gradient formation occurred within 30–60 s after placing the dye solution in the sample reservoir with the majority of the delay due to the time required for the sample channel to fill with

dye. Once sample solution reached the intersection, the chemoattractant entered the cell channel as a plume. We estimate that 0.24 s was required for xylose to penetrate the cell channel depth, based on a bulk diffusion coefficient, $D_{xylose}$,[48] of $7.5 \times 10^{-6}$ $cm^2/s$ and a channel depth of 19 μm. With a linear velocity of 15–30 μm/s in the cell channel, xylose was carried 4–7 μm downstream of being introduced before reaching a uniform concentration across the cell channel. Due to rapid diffusion across the cell channel, the gradient had a steep rising edge (i.e., step), and beyond this point, cells no longer experienced a concentration gradient.

This work utilized the smallest diameter pores possible without substantially affecting xylose diffusion[49,50] to ensure that gradient formation was controlled primarily by diffusion rather than pressure-driven flow across the membrane. Because the volumetric flow rate from hydrostatic transport scales as the fourth power of the pore radius,[51] decreasing pore diameter dramatically decreases hydrostatic transport through the membrane. For a typical transmembrane pressure of ~1 mm $H_2O$, we estimate a volumetric flow rate through the membrane of ~20 aL/s into a total intersection volume of 230 pL and a microchannel volumetric flow rate of ~50 pL/s. Similar devices constructed with membranes containing 50 nm, 1 μm, and 2 μm diameter pores were more susceptible to variation in pressure across the membrane and showed considerably more variability in sample transport over time and from device to device (data not shown). For 10 nm diameter pores, however, hydrostatic flow across the membrane was minimal, resulting in a stable gradient that was readily reproduced from device to device.

To quantify gradient stability, we calculated a dilution ratio, representing the fluorescence in the cell channel at the intersection relative to the fluorescence in the sample channel, with Equation 1,

$$dilution\ ratio = \frac{s_{\text{int}} - s_{sample}}{s_{sample} - b} \tag{1}$$

where $s_{int}$ was the fluorescence signal at the intersection, $s_{sample}$ was the fluorescence in the sample channel, and $b$ was background from membrane auto-fluorescence. For constant fluid levels in the reservoirs, the dilution ratio was 0.09 and extremely stable with a relative standard deviation (RSD) of ~0.5% over 30 min. Exchange of the solution in the sample inlet (reservoir 4) during the course of an experiment increased the deviation in the dilution ratio to an RSD of ~13% over 30–60 min. This level of variation is acceptable for experiments such as those reported here which vary chemoattractant concentrations over orders of magnitude. The RSD for the average dilution ratio was 16% for n = 29 devices, indicating good repeatability from device to device. The fact that device-to-device variation was comparable to the variability of a single device over the course of an experiment was important because data from multiple devices on different days could be pooled or compared. Unfortunately, most previous reports of membrane-based devices have not quantified gradient stability over time or reproducibility from device to device, making a direct comparison to prior art[30,31,36] difficult.

## Cell swimming in the device

Conditions in the microfluidic device were chosen to maintain cell viability and motility. The PDMS substrates were only ~1.5 mm thick to allow gas exchange through the PDMS and permitted the strictly aerobic cells to survive long term in the microchannels. In fact, cell growth and motility can persist for up to 24 h within the microfluidic device. For the chemotaxis and motility studies, the swarmer cells were collected and assayed in their

growth medium, M2G, which contained glucose as a carbon source. Finally, a gentle hydrostatic flow rates between 15 – 30 μm/s were used so that the *C. crescentus* swarmer cells could easily swim upstream and control their position within the channel. A video of cells swimming in the device is included in the Supporting Information.

Figure 3 shows representative results for the cell video data, cell tracking plug-in, and MATLAB trajectory analysis. Figure 3a is a composite fluorescence image in which each pixel shown is the maximum value recorded at that position during the video. The distance traveled between frames was greater for swimming swarmer cells than for non-swimming cells (straight, bright streaks), demonstrating that the hydrostatic flow did not impede swarmer cell motility. The average cell velocities with and without hydrostatic flow are comparable and are discussed below. Figure 3b shows the results of the ParticleTracker plug-in for this video with individual trajectories shown in different colors. Comparison of panels (a) and (b) in Figure 3 shows that the ParticleTracker plug-in[43] accurately identified the coordinates of individual bacterial trajectories. Figure 3c depicts a MATLAB plot of the white trajectory in Figure 3b. A green dot marks the start of the trajectory, a red dot marks the end, and blue dots indicate turns identified by the MATLAB program.

The trajectory in Figure 3c demonstrates that the custom MatLab program was capable of identifying turns and discriminating these abrupt changes in trajectory from circular swim patterns. Bacteria follow circular paths when in close proximity to a surface,[52,53] and this behavior was frequently observed during these experiments. In this work, turns caused by flagellar reversal were used as a metric for chemotaxis. Because circular swimming does not involve reversal of flagellum rotation, and therefore, is not directly indicative of chemotaxis, accurate analysis by the MatLab program was critical to distinguish between turns and circular paths. However, because chemoattractant concentration in the cell channel was highest at the membrane surface, circling may reflect chemotaxis indirectly: cells moved up the chemoattractant gradient toward the surface and therefore exhibited circular swimming. Future work will investigate whether an increase in circular swim patterns is correlated with the presence of chemoattractant. Additionally, although other species of bacteria turn by tumbling or by temporarily stopping flagellar rotation, the software should still identify these motions as abrupt turns, making it applicable to future work with a wide range of flagellated organisms.

Individual experiments typically lasted between 30–60 min and included several hundred trajectories. For example, studies with wild type cells averaged 430 trajectories per 30–60 min long experiment. During the course of an experiment, control observations were performed on the same device and with the same population of cells as the experimental observations. Additionally, once a concentration eliciting a chemotactic response had been identified, subsequent experiments included this concentration as a positive control. The rapidity of gradient formation was critical in measuring three or more conditions on the same cell population because the duration of each experiment was limited by the life cycle of *C. crescentus*. After approximately 30–60 min at room temperature, the enriched swarmer cells enter the stalked phase of their life cycle (Figure S-1) and become non-motile and subsequently incapable of chemotaxis.

While data collection typically lasted between 30–60 min, data analysis with the ParticleTracker plug-in and MATLAB required approximately 2 h. The majority of this time was spent determining coordinates for individual cell trajectories. Improvement in cell tracking calculations and further automation of the data processing will greatly reduce the time required for this analysis. Additionally, the number of cells analyzed during an experiment was limited by the maximum cell density compatible with accurate trajectory determination. At higher cells densities, the ParticleTracker plug-in failed to track accurately

cells that crossed paths. Consequently, improved tracking software could potentially permit increased cell densities in addition to faster analysis times, resulting in higher throughput.

To increase sample sizes in the current work, data were collected from multiple experiments over several days, and the lengths and durations of all runs were compiled. Data summation was possible because of the high device-to-device reproducibility discussed above. For each strain and condition, between 162 and 1161 trajectories were analyzed. Of these, ~40% contained at least one run nested between two turns, and the compiled data for each condition included between n = 143 and n = 1050 runs. A summary of the number of runs and average length and duration for each condition is given in Tables S-1 and S-2 in the Supporting Information. Due to the large variation in run length and duration and the skew of the data, we chose to present the results as histograms (see Figures 4–5). Both the run length and run duration distributions have maximal observation counts in the minimum value bins and taper off at higher values. The distributions of run length and duration for a given condition are similarly shaped, and the average cell velocity during the runs, ~30 μm/s, was fairly constant. The average cell velocities with and without hydrostatic flow were also similar. The data in Figure 5 show an average velocity of 34 μm/s for the wild type cells and 29 μm/s for the chemotaxis-impaired mutant cells with a supplemental hydrostatic flow of 15–30 μm/s, whereas the average velocity for the wild-type cells without hydrostatic flow present was 32 μm/s.

## Chemotaxis assays of the wild type cells

For the wild type cells, the average run length and run duration were 68 μm and 2.0 s, respectively, in the absence of a xylose gradient. Exposure to the xylose gradients resulted in a 20–40% decrease in average run length and a 15–25% decrease in average run duration (see Table S-1). The turn frequency observed in these experiments was higher than previously reported for *C. crescentus*; for example, one literature report gives an average of ~0.5 turn every 5 s.[19] Previous work has shown that confinement in micrometer-scale channels affects cell motion in *E. coli*,[54,55] and for the experiments reported here, a number of turns occurred when a cell approached the channel wall and then changed direction. This effect may have increased the turn frequency observed.

In the presence of a xylose gradient, the proportion of short (≤ 25 μm and ≤ 1 s) runs increased. This is evident in the normalized histograms in Figure 4 as an increase in the frequency of observations in the minimum value bins for the xylose-treated runs compared to the control. This indicates a chemotactic response as the cells increased the number of rapid course corrections to stay near the patch of xylose at the intersection. The intersection was 110 μm of the 410 μm long field of view, so runs much longer than 110 μm would likely move a cell down the concentration gradient. Because movement down a chemoattractant gradient increases turn frequency,[6] we expect the presence of a xylose gradient at the intersection to decrease the proportion of longer runs, as observed. To control for the effects of time spent in the device and the exchange of reservoir contents, experiments were performed in which the sample reservoir was refilled with fresh M2G rather than a xylose solution. These experiments showed no significant change in cell behavior induced by the time spent in the device or the exchange of reservoir contents (unpaired t-tests, $p = 0.75$ for run length and 0.76 for run duration; data not shown).

To determine whether the change in behavior with xylose treatment seen in Figure 4 was statistically significant, a one-way analysis of variance (ANOVA) and a Tukey means comparison were performed in OriginPro 8.0 (OriginLab Corp.). Prior to these statistical analyses, we applied a log-transformation to obtain normally distributed data in compliance with the assumptions of these parametric statistical tests. The ANOVAs showed a significant difference between the means ($p < 0.001$ for both length and duration), and the means

comparison test established that the three highest xylose concentrations tested (130 μM, 13 mM, and 1.3 M) each differed significantly from the control, while the lowest xylose concentration (1.3 μM) did not.

The sensitivity of this assay depends on both the response of *C. crescentus* to a given concentration and gradient and on the quantity of data taken. Owing to inherent variability in run length and duration, empirical observations provide only inexact measurements of the true underlying bacterial behavior for a particular condition. For a given number of observations, statistical tests may thus fail to identify small (but real) changes in behavior, whereas larger sample sizes increase confidence in the measured estimators and permit statistically significant identification of smaller effects. A statistical power analysis (see Supporting Information) shows that the 143 observations in the 1.3 μM xylose treatment provide sufficient sensitivity to successfully detect behavioral decreases of at least 26 μm in run length or 0.52 s in run duration with 90% confidence. For the 143 experimental runs, we observed decreases of only 14 μm in run length and 0.4 s in run duration. Consequently, the absence of a significant difference between the 1.3 μM xylose treatment and the control could indicate either an absence of chemotactic behavior or an effect too small to detect based on our sample size.

Interestingly, statistically significant differences in swimming behavior were not observed between the different xylose concentrations, and the histograms in Figure 4 show similar changes for concentrations spanning four orders of magnitude (130 μM to 1.3 M). Bacterial chemotaxis is robust across a wide range of chemoattractant concentrations because of regulatory feedback based on methylation of the chemoreceptors.[7] As a result, cells respond sensitively to the relative steepness of a chemical gradient rather than to the absolute concentration at their location, and an absence of correlation between xylose concentration and swimming behavior is not unexpected if the gradient is similarly shaped for all concentrations. As discussed above, attempts at confocal imaging of the gradient were unsuccessful, and we were not able to confirm the shape of the gradient at each concentration. However, the MPTS data suggest the material transport is similar over a broad concentration range.

### Chemotaxis and motility assays of the chemotaxis-impaired mutant

We also examined the swimming behavior of a chemotaxis-impaired mutant, CB15Δ*cheA*, as a control. In these cells, the *cheA* gene has been removed by in-frame deletion. Deletion of *cheA* allows chemoattractant binding to the receptor outside the cell, but abolishes the subsequent switching of flagellum motor rotation and therefore should impair chemotaxis toward all attractants.[6,7] Indeed, the chemotaxis-impaired cells showed no significant change in either run length or run duration in the presence of 130 μM, 13 mM, or 1.3 M xylose (one-way ANOVA p-values = 0.11 for length and 0.18 for duration), and a two-way ANOVA demonstrated a statistically significant difference between the wild type response and the mutant response to xylose (interaction p-value < 0.01 for both length and duration). Histograms of the data for the mutant are included in the Supporting Information as Figure S-5.

Interestingly, the baseline cell swimming behavior for the Δ*cheA* strain differed markedly from that of the wild type cells. The chemotaxis-impaired cells had an average run length of 41 μm and an average run duration of 1.4 s, compared to 68 μm and 2.0 s for the wild type cells. Figure 5 shows histograms of run length and run duration for the wild type and chemotaxis-impaired cells. Similar to the xylose-treated wild type cells, the chemotaxis-impaired mutant shows a high proportion of short runs compared to the wild type control. In fact, the Δ*cheA* mutant exhibited a larger fraction of shorter runs than those of the xylose-

treated wild type cells, which had average run lengths and durations ranging from 42–55 μm and 1.5–1.7 s, respectively (see Table S-1).

The data in Figure 5 indicate that deletion of *cheA* in *C. crescentus* causes an increase in the frequency of switching of the flagellum motor. This is surprising because deletion of *cheA* in several species related to *C. crescentus* results in smooth-swimming.[7,56–59] This intriguing observation suggests the mechanism underlying chemotaxis in *C. crescentus* may differ substantially from what has been previously reported among the Gram negative bacteria. The difference in swimming behavior between wild type and Δ*cheA* strains could only have been detected by single cell trajectory measurements. Traditional chemotaxis assays, such as the swarm plates in Figure S-2, do not yield this type of information.

## Conclusions

The observation that the wild type and Δ*cheA* strains exhibit different baseline swimming patterns demonstrates the utility of microfluidic platforms to studies of bacterial motility in general and the importance of single cell studies in obtaining certain types of information. The micrometer to millimeter dimensions of microchannels match well with a microscopic field of view and allow individual cells to be monitored over useful time scales (in this case, tens of seconds). The macroscopic measurements used in most traditional chemotaxis assays[60,61] would not have reflected this difference in the microscopic behavior of the cells.

These results also demonstrate the utility of microchannel-nanopore devices for rapid formation of a stable, reproducible chemical gradient for chemotaxis studies. The nanopore membranes in these devices are commercially available, the fabrication methods used are inexpensive, and operation of the device is straightforward, requiring no pumps or valves, only hydrostatic pressure. These advantages should help to make these devices more accessible to non-specialists. While more sophisticated devices produce more complex gradients, the device presented here is advantageous for rapid screening and could be used to quickly establish potential attractants and relevant concentrations for further study.

## Supplementary Material

Refer to Web version on PubMed Central for supplementary material.

## Acknowledgments

The authors thank Prof. Daniel B. Kearns for helpful discussions, John M. Perry for providing a data reformatting program, and Andrew S. Wilkens for the cell velocity measurements without hydrostatic flow. This work has been supported in part by NSF CHE-0750295 for SCJ, by NIH GM077648 and NIH GM51986 for YVB, by the Indiana METACyt Initiative of Indiana University, funded in part through a major grant from the Lilly Endowment, Inc., and by a fellowship from Merck Research Laboratories for MLK. PJBB and DTK are supported by postdoctoral National Institutes of Health National Research Service Awards number F32A1072993 from the National Institute of Allergy and Infectious Diseases (PJBB) and number F32GM083581 from the National Institute of General Medical Sciences (DTK).

## References

1. Rao CV, Ordal GW. Trends Microbiol. 2008; 16:408–487.
2. Szurmant H, Ordal GW. Microbiol Mol Biol Rev. 2004; 68:301–319. [PubMed: 15187186]
3. Alley MRK, Gomes SL, Alexander W, Shapiro L. Genetics. 1991; 129:333–342. [PubMed: 1660425]
4. Miller LD, Russell MH, Alexandre G. Adv Appl Microbiol. 2009; 66:53–75. [PubMed: 19203648]
5. Wadhams GH, Armitage JP. Nat Rev Mol Cell Biol. 2004; 5:1024–1037. [PubMed: 15573139]

6. Stock, JB.; Surette, MG. Escherichia coli and Salmonella typhimurium: Cellular and molecular biology. Neidhardt, FC., editor. ASM Press; Washington, DC: 1996. p. 1103-1129.
7. Baker MD, Wolanin PM, Stock JB. Curr Opin Microbiol. 2006; 9:187–192. [PubMed: 16529985]
8. Pandey J, Chauhan A, Jain RK. FEMS Microbiol Rev. 2009; 33:324–375. [PubMed: 19178567]
9. Pandey G, Jain RK. Appl Environ Microbiol. 2002; 68:5789–5795. [PubMed: 12450797]
10. Parales RE, Harwood CS. Curr Opin Microbiol. 2002; 5:266–273. [PubMed: 12057680]
11. Poindexter JS. Bacteriol Rev. 1964; 28:231–295. [PubMed: 14220656]
12. Inagaki F, Takai K, Hirayama H, Yamato Y, Nealson KH, Horikoshi K. Extremophiles. 2003; 7:307–317. [PubMed: 12743833]
13. Mannisto MK, Tiirola MA, Salkinoja-Salonen MS, Kulomaa MS, Puhakka JA. Arch Microbiol. 1999; 171:189–197. [PubMed: 10201097]
14. Hu P, Brodie EL, Suzuki Y, McAdams HH, Andersen GL. J Bacteriol. 2005; 187:8437–8449. [PubMed: 16321948]
15. Ji GY, Salzberg SP, Silver S. Appl Environ Microbiol. 1989; 55:523–525. [PubMed: 2655538]
16. Braz VS, Marques MV. FEMS Microbiol Lett. 2005; 251:289–295. [PubMed: 16168577]
17. Hillson NJ, Hu P, Andersen GL, Shapiro L. Appl Environ Microbiol. 2007; 73:7615–7621. [PubMed: 17905881]
18. Patel J, Zhang Q, McKay RML, Vincent R, Xu Z. Appl Biochem Biotechnol. 200910.1007/s12010-12009-18540-12010
19. Ely B, Gerardot CJ, Fleming DL, Gomes SL, Frederikse P, Shapiro L. Genetics. 1986; 114:717–730. [PubMed: 3792824]
20. Mao H, Cremer PS, Manson MD. Proc Natl Acad Sci. 2003; 100:5449–5454. [PubMed: 12704234]
21. Nam SW, Van Noort D, Yang Y, Park S. Lab Chip. 2007; 7:638–640. [PubMed: 17476385]
22. Jacobson SC, McKnight TE, Ramsey JM. Anal Chem. 1999; 71:4455–4459.
23. Dertinger SKW, Chiu DT, Jeon NL, Whitesides GM. Anal Chem. 2001; 73:1240–1246.
24. Amarie D, Glazier JA, Jacobson SC. Anal Chem. 2007; 79:9471–9477. [PubMed: 17999467]
25. Mosadegh B, Huang C, Park JW, Shin HS, Chung BG, Hwang SK, Lee KH, Kim HJ, Brody J, Jeon NL. Langmuir. 2007; 23:10910–10912. [PubMed: 17910490]
26. Lanning LM, Ford RM, Long T. Biotechnol Bioeng. 2008; 100:653–663. [PubMed: 18306417]
27. Long T, Ford RM. Environ Sci Technol. 2009; 43:1546–1552. [PubMed: 19350933]
28. Seymour JR, Ahmed T, Marcos Stocker R. Limnol Oceanogr: Methods. 2008; 6:477–488.
29. Ahmed T, Stocker R. Biophys J. 2008; 95:4481–4493. [PubMed: 18658218]
30. Diao J, Young L, Kim S, Fogarty EA, Heilman SM, Zhou P, Shuler ML, Wu M, DeLisa MP. Lab Chip. 2006; 6:381–388. [PubMed: 16511621]
31. Cheng S-Y, Heilman S, Wasserman M, Archer S, Shuler ML, Wu M. Lab Chip. 2007; 7:763–769. [PubMed: 17538719]
32. Park J, Bansal T, Pinelis M, Maharbiz MM. Lab Chip. 2006; 6:611–622. [PubMed: 16652176]
33. Salman H, Zilman A, Loverdo C, Jeffory M, Libchaber A. Phys Rev Lett. 2006; 97:118101. [PubMed: 17025931]
34. Abhyankar VV, Lokuta MA, Huttenlocher A, Beebe DJ. Lab Chip. 2006; 6:389–393. [PubMed: 16511622]
35. Keenan TM, Hsu C-H, Folch A. Appl Phys Lett. 2006; 89:114103.
36. Kim D, Lokuta MA, Huttenlocher A, Beebe DJ. Lab Chip. 2009; 9:1797–1800. [PubMed: 19495465]
37. Ismagilov RF, Ng JMK, Kenis PJA, Whitesides GM. Anal Chem. 2001; 73:5207–5213. [PubMed: 11721920]
38. Cannon DMJ, Kuo T-C, Bohn PW, Sweedler JV. Anal Chem. 2003; 75:2224–2230. [PubMed: 12918959]
39. Zhou K, Kovarik ML, Jacobson SC. J Am Chem Soc. 2008; 130:86148616.
40. Degnen ST, Newton A. J Mol Biol. 1972; 64:671–680. [PubMed: 5022192]
41. Koch B, Jensen LE, Nybroe O. J Microbiol Methods. 2001; 45:187–195. [PubMed: 11348676]

42. Johnson RC, Ely B. Genetics. 1977; 86:25–32. [PubMed: 407126]
43. Sbalzarini IF, Koumoutsakos P. J Struct Biol. 2005; 151:182–195. [PubMed: 16043363]
44. Schmidt JM. J Gen Microbiol. 1966; 45:347–353. [PubMed: 5969754]
45. Bodenmiller D, Toh E, Brun YV. J Bacteriol. 2004; 186:1438–1447. [PubMed: 14973013]
46. Roman GT, Hlaus T, Bass KJ, Seelhammer TG, Culbertson CT. Anal Chem. 2005; 77:1414–1422. [PubMed: 15732926]
47. Xia P, Bungay PM, Gibson CC, Kovbasnjuk ON, Spring KR. Biophys J. 1998; 74:3302–3312. [PubMed: 9635784]
48. Ueadaira H, Uedaira H. Bull Chem Soc Jpn. 1969; 42:2140–2142.
49. The ratio of solute to nanopore radius was 0.065, meaning that the apparent diffusion coefficient of xylose through the membrane should be roughly 90% of the bulk diffusion coefficient and contributions of steric hindrance to diffusive transport through the membrane were minimal. While hindered diffusion was likely negligible for a small molecule chemoattractant such as xylose, this effect should be considered when choosing nanopore dimensions for larger putative attractants, e.g., peptides.
50. Deen WM. AIChE J. 1987; 33:1409–1425.
51. Giddings, JC. Unified separation science. Wiley-Interscience; New York: 1991.
52. Frymier PD, Ford RM, Berg HC, Cummings PT. Proc Natl Acad Sci. 1995; 92:6195–6199. [PubMed: 7597100]
53. Lauga E, DiLuzio WR, Whitesides GM, Stone HA. Biophys J. 2006; 90:400–412. [PubMed: 16239332]
54. Liu Z, Papadopoulos KD. Appl Environ Microbiol. 1995; 61:3567–3572. [PubMed: 7486991]
55. Hill J, Kalkanci O, McMurry JL, Koser H. Phys Rev Lett. 2007; 98:068101. [PubMed: 17358984]
56. Hyakutake A, Homma M, Austin MJ, Boin MA, Hase CC, Kawagishi I. J Bacteriol. 2005; 187:8403–8410. [PubMed: 16321945]
57. McCarter LL. Microbiol Mol Biol Rev. 2001; 65:445–462. [PubMed: 11528005]
58. Porter SL, Wadhamns GH, Armitage JP. Trends Microbiol. 2008; 16:251–260. [PubMed: 18440816]
59. Schmitt R. Microbiol. 2002; 148:627–631.
60. Adler J. Science. 1966; 153:708–716. [PubMed: 4957395]
61. Adler J. J Gen Microbiol. 1973; 74:77–91. [PubMed: 4632978]

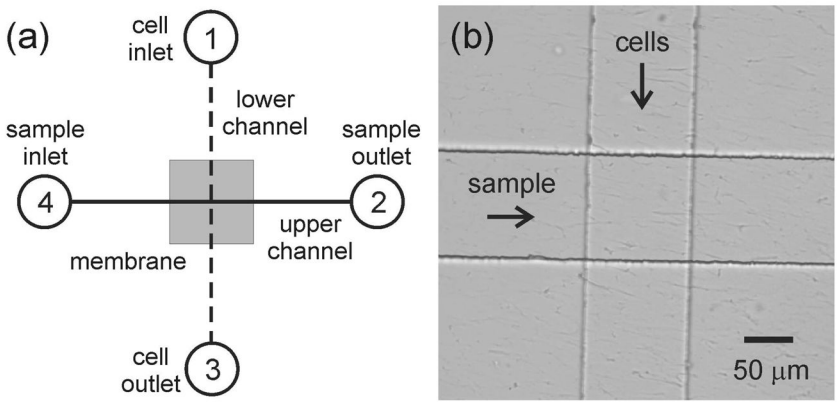


**Figure 1.**
(a) Schematic of the microchannel-nanopore device. (b) White light image of the intersection of the two microchannels bridged by a track-etched membrane with 10 nm diameter pores. The vertical cell channel is in the lower layer, and the horizontal sample channel is in the upper layer.

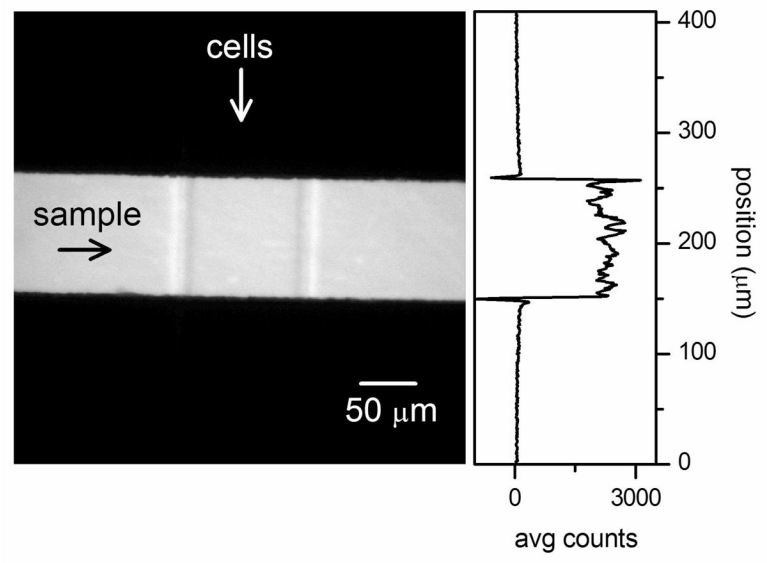


**Figure 2.**

Fluorescence image of 8-methoxypyrene-1,3,5-trisulfonic acid (MPTS) at the microchannel intersection. The horizontal sample channel was filled with 10 μM MPTS in M2G, and the vertical cell channel was filled with M2G without dye. The line profile to the right shows the average fluorescence along the length of the cell channel with the background fluorescence from the membrane and sample channel subtracted.

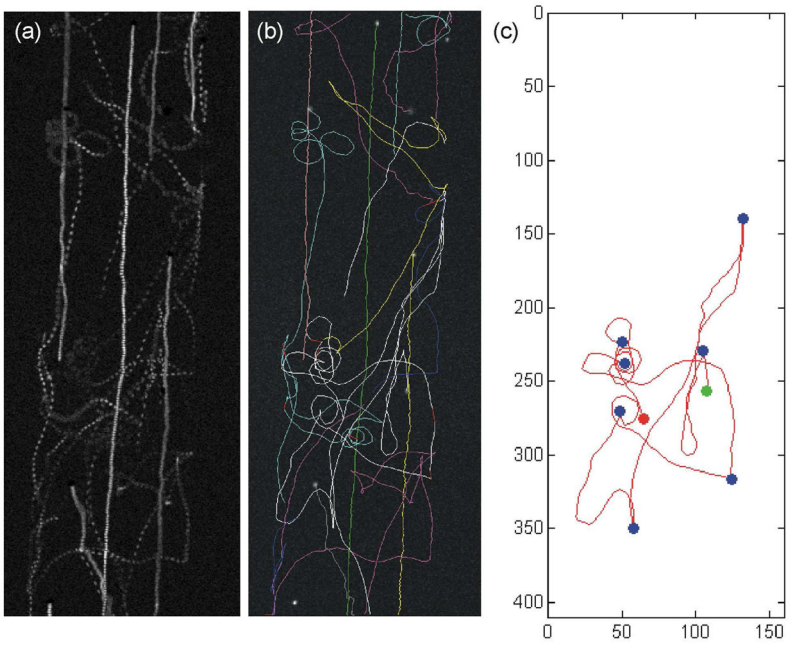


**Figure 3.**

(a) A composite fluorescence image of cells in the device obtained from the brightest pixel at each location during a 301 frame video. The video used to produce this image is included in the Supporting Information. (b) Trajectories identified by the ParticleTracker plug-in for ImageJ for the video data shown in (a). (c) A MATLAB plot of the white trajectory from (b) with the start, end, and turn locations identified with green, red, and blue dots, respectively. The axis labels in (c) are in micrometers, and the scale is the same for all panels.

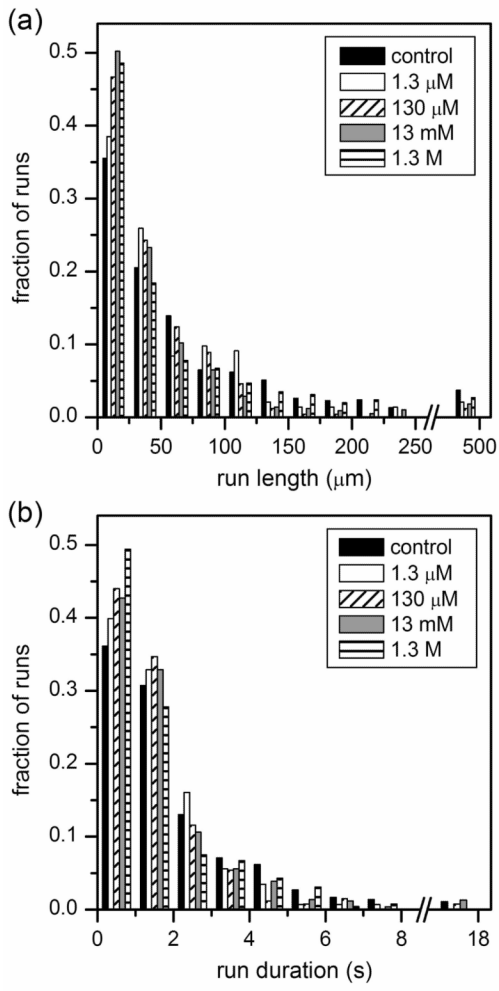


**Figure 4.**

Histograms of (a) run length and (b) run duration distributions for a control, in which the sample channel was filled with M2G, and for xylose concentrations of 1.3 μM, 130 μM, 13 mM, and 1.3 M. For both run length and duration, the 130 μM, 13 mM, and 1.3 M xylose concentrations were statistically different from the control. Note breaks in x-axes: the last bin contains runs with 250 μm < length ≤ 500 μm in (a) and 8 s < duration ≤ 18 s in (b).

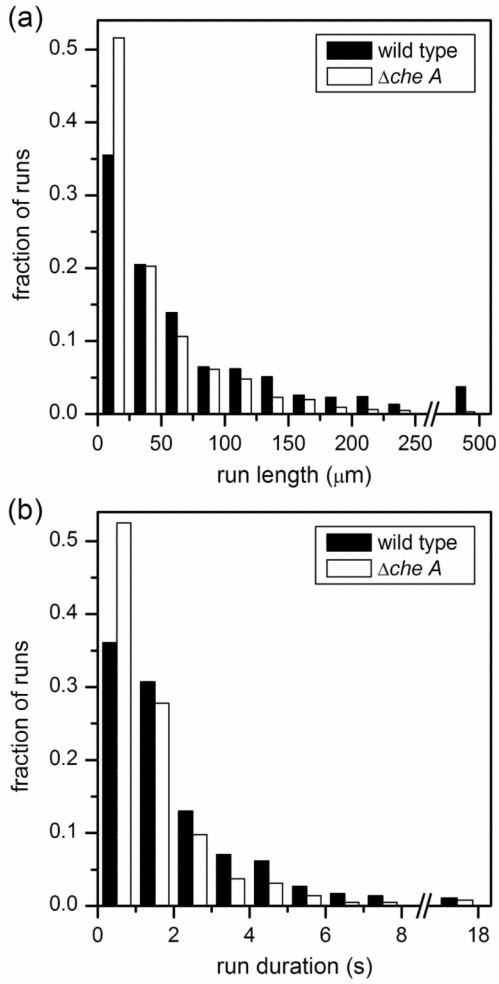


**Figure 5.**

Histograms of (a) run length and (b) run duration distributions for wild type cells and for a chemotaxis-impaired mutant (Δ*cheA* in the legend). In both cases the sample channel was filled with M2G. Note breaks in x-axes: the last bin contains runs with 250 μm < length ≤ 500 μm in (a) and 8 s < duration ≤ 18 s in (b).